J. Fluid Mech. (1987), *vol.* 181, *pp.* 141–161
Printed in Great Britain

Nonlinear interaction and the transition to turbulence in the wake of a circular cylinder

By A. KOURTA, H. C. BOISSON, P. CHASSAING AND H. HA MINH

Institut de Mecanique des Fluides de Toulouse, Laboratoire associé au C.N.R.S. LA 0005, 2, rue Charles Camichel, 31071 Toulouse, France

(Received 2 January 1986 and in revised form 24 December 1986)

The transition and the development of turbulence in the near wake of a circular cylinder are investigated using hot-wire anemometry and flow visualization. The formation zone of the large regular vortices is studied in the subcritical regime ($2000 < U_0 D/\nu < 60000$), with and without the introduction of a splitter plate. Two different regimes are identified in the interaction between the von Kármán vortices and those of the shear layer emerging from the separated boundary layer. Experimental evidence is given in support of the strong coupling at low Reynolds numbers characterized by phase modulations between the two types of structures. The interaction is weaker at high Reynolds numbers where the small-scale vortices are disconnected from the regular vortex shedding, giving rise to an intermittent pattern. Spectral properties are used to describe the different stages of the interaction between the shear-layer vortices and the alternating ones. Physical properties of the interaction are examined separately in a numerical simulation using a pressure–velocity formulation. Both unexcited and excited two-dimensional plane mixing layers are studied using streakline maps and time traces of the dynamical properties. The main features of the simulated vortex development are in agreement with the experimental results.

1. Introduction

Examples of macroscopic organized structures in the first stages of transition to turbulence are numerous in fluid dynamics. These structures are found to be the consequence of well-known instability mechanisms. In the case of incompressible fluids, the so-called instabilities of Taylor–Couette, Rayleigh–Bénard or Kelvin–Helmholtz have been widely studied and review studies are respectively provided by Busse (1981), Di Prima & Swinney (1981) and Ho & Huerre (1984).

Recent work on dynamical systems has shown the importance of early organized periodic structures in deterministic chaos and the possible occurrence of random-like motions with a limited number of degrees of freedom. Comparisons between these theories and experimental cases have been pointed out by Eckmann (1981), among others. The power spectra of such systems exhibit one, then two and possibly three independent basic frequencies. Simultaneously a broadband noise is observed, which corresponds to the occurrence of chaos in the sense of the theoretical scenario established by Newhouse, Ruelle & Takens (1978).

The present work is mainly devoted to describing such mechanisms of turbulence in the near wake of a circular cylinder by interaction between vortical motions of different scales.

For the low Reynolds-number range of 36 to 200, Sreenivasan (1985) found that the chaos appears in the wake after a quasi-periodic regime resulting from two or more independent frequencies, the vortex shedding one being the basic periodicity. When the Reynolds number is increased, a more complicated quasi-periodic pattern is observed with the occurrence of other basic frequencies and successively chaos and quasi-periodicity are found. A theoretical analysis of the von Kármán vortex trail by Sirovich (1985) shows that the vortex shedding is the driving mechanism that creates both the vortex street and the perturbations. In this case additional frequencies are found and can be related to the successive states observed by Sreenivasan (1985).

In the present paper, the subcritical regime is examined ($2000 < R < 60000$). The flow pattern is different, since two distinct sources of periodic structures can be identified:

(i) The existence of a well-defined pseudoperiodic motion at the wake vortex-shedding frequency, up to high Reynolds numbers is well known. The experimental works of Kovasznay (1959) and Roshko (1954) have given a global description of the phenomenon in both laminar and turbulent regimes. The more recent works of Cantwell (1976), Wlezien & Way (1979), Owen & Johnson (1980) and Boisson, Chassaing & Ha Minh (1983) have provided details on the organized motion in the near wake, educed from the virtually turbulent fine-scale motion.

(ii) Some experimentalists have also pointed out the presence of two-dimensional Tollmien–Schlichting waves and their rolling up into small vortices in the mixing layer emerging from the cylinder. Crausse (1936) reported on this phenomenon, providing flow visualizations.

Roshko (1954) observed that the transition occurs in the separated boundary layer at sufficiently high subcritical Reynolds numbers, all large-scale shedding vortices once formed being turbulent. Gerrard (1966) pointed out the role of the formation region and the mixing layers in which he observed the transition.

Bloor (1964) discussed the influence of the Reynolds number on the position of the transition point and on the frequency of the transitional vortices in the mixing layer. She established that this point moves upstream as the Reynolds number increases and the ratio of the mixing-layer frequency to the vortex-shedding one is proportional to $R^{\frac{1}{2}}$, R being the Reynolds number based upon the free-stream velocity and the diameter of the cylinder ($4000 < R < 16000$).

Using different fluids and different cylinder diameters other experimentalists have reported on this phenomenon, and flow visualizations from Domptail (1979) and Jones, Barbi & Telionis (1981) corroborate these results. However, Wei & Smith (1986), using both flow visualizations and hot-film anemometry in a water channel, established that the frequency ratio demonstrates a 0.87 power-low relationship with respect to the Reynolds number, contrary to the 0.5 reported by Bloor (1964).

The previous results suggest that the transitional process in the near wake is mainly governed by the interaction between the vortices originating from two basic configurations: (i) the wake; and (ii) the mixing layer. Both of these are reputed to be initially two-dimensional. Moreover, it appears that these vortical structures, once in existence, have a significant signature in the frequency spectra. Thus the transition mechanism associated with the spectral broadening should be characterized by interactions between frequencies.

The aim of this study is to provide circumstantial information on the establishment of the chaos from a detailed analysis of the spectral shapes and the physical description of the interacting structures. The different phases of transition to a

chaotic behaviour are observed at different spatial positions in the flow for different Reynolds numbers.

Two complementary means have been used to shed some light on the mechanisms of vortex interaction in the mixing layers of the formation region: an experimental approach and a numerical simulation.

The experimental study is mainly based upon hot-wire anemometry measurements and spectral analysis. These are complemented by flow visualizations using schlieren techniques and high-speed-film camera frames.

In order to separate the properties due to the vortex shedding from those due to the mixing layer, the cylinder is fitted with a wake splitter plate along the x-axis. The same effects on drag or the base pressure coefficient observed by Apelt, West & Szewczyk (1973), Bearman (1965) and Gerrard (1966) are also found here and the vortex shedding process is very significantly modified. Results obtained in the mixing layer are therefore compared with and without a plate.

The Reynolds-number range from 2000 to 60000 is investigated. Two flow regimes can be distinguished as shown by Kourta *et al.* (1985*b*). They are described in §3.1 on the basis of detailed measurements. Sections 3.2, 3.3 and 3.4 are devoted to the nature of the strong interaction between frequencies with and without a splitter plate, in the lower Reynolds-number range (first regime) and §3.5 deals with the higher Reynolds-number range (second regime).

The last part of this paper is devoted to the study of the governing mechanism in the initial mixing layer simulated from a numerical solving of the two-dimensional unsteady Navier–Stokes equations. It involves a simplification of the actual flow configuration in order to focus on the two-dimensional interaction, which can be predominant compared to spanwise three-dimensional perturbation in the initiation of chaotic behaviour.

2. Apparatus and measurements

The experiments are conducted in a return-circuit wind tunnel as described by Boisson *et al.* (1981), Boisson (1982) and Kourta (1984). A convergent section with a contraction ratio of 11 following a set of five smoothing screens ensures a uniform velocity profile at the entrance of the test section and a turbulence level of less than 0.1 %. These characteristics are maintained throughout the whole test volume by a slowly diverging section. The nominal dimensions are 70 cm in the vertical direction, 60 cm along the transverse direction and 190 cm in the horizontal direction.

A polyvinyl chloride (PVC) cylinder of diameter $D = 42$ mm vertically spans the test section 30 cm from the entrance.

The origin of the coordinates is taken at the centre of the cylinder midway between the tunnel floor and the roof. The x-axis coincides with the direction of the flow, the z-axis with the cylinder axis, and the y-direction is normal to these two.

End plates are added in order to minimize the interaction between the cylinder and the tunnel boundary layers and to obtain a two-dimensional mean flow, as suggested by the results of Stansby (1974). The plates are designed according to his prescriptions and have the same geometry as that used by West & Apelt (1982) (figure 1). The two-dimensional character of the mean flow is tested by measuring the value of C_{pb} (the base pressure coefficient) in the spanwise direction. These values are found to be constant within an accuracy of 2 % over more than 85 % of the cylinder.

A preliminary investigation shows that the value of C_{pb} is reduced when adding the end plates. This was shown to correspond to a reduction of the near-wake lateral

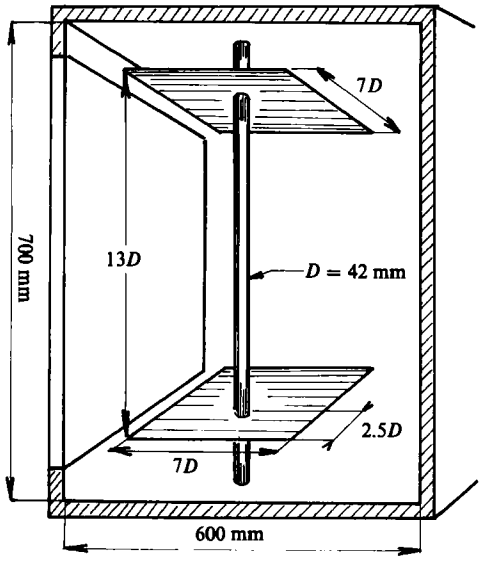

FIGURE 1. The working section and the cylinder with end plates.

dimension. Although the aspect ratio L/D is reduced from 16 to 13, this effect should not be attributed to these variations, as shown by the results of West & Apelt (1982) for comparable values of this parameter. The reduction of the base pressure coefficient, and thus of the wake lateral dimension, is probably caused by the decreased inflow at the ends owing to the fitting of the end plates. In this case the blockage is equal to 6.7 %.

Measurements are made using single tungsten hot-wire probes (5 μm and 9 μm) parallel to the cylinder axis. The 9 μm probe is better adapted to the very low velocity in the wall region and thus was used for all the measurements in the shear layers. The probes are monitored by constant-temperature anemometers, DISA 55M10 with 55D10 linearizers. As the spanwise velocity is supposed to be negligible, the hot-wire signal merely represents the modulus of the velocity vector. This type of probe is chosen in order to obtain an optimal spatial resolution as the wall is approached. The positioning of the probe is computer controlled with a repeatability of 10 μm.

The anemometers are connected to a PLURIMAT-S-400 computer via 48 dB/octave filters to avoid aliasing. An analog/digital converter (12 bits) is used and the sampling frequency (f_e) for these experiments varies from 200 Hz to 10 KHz. Typically, N blocks of M samples ($N = 50$; $M = 2048$) are used for the statistical calculations (probability density function, power spectra or phase averages).

An estimate of the probability density function is obtained by computing the amplitude histograms of the signal. The spectra are calculated using a fast-Fourier-transform algorithm applied to the raw signal of a block and averaging the corresponding spectral power. The frequency resolution is then defined as $df = f_e/N$ and varies from 0.244 to 4.88 Hz.

In order to restore the properties of the main vortex shedding, a phase-averaging technique, similar to the one used by Boisson *et al.* (1983) is applied. As shown in the following, this analysis is restricted to high Reynolds numbers where the background motion of small vortices can be considered as a random noise uncoupled

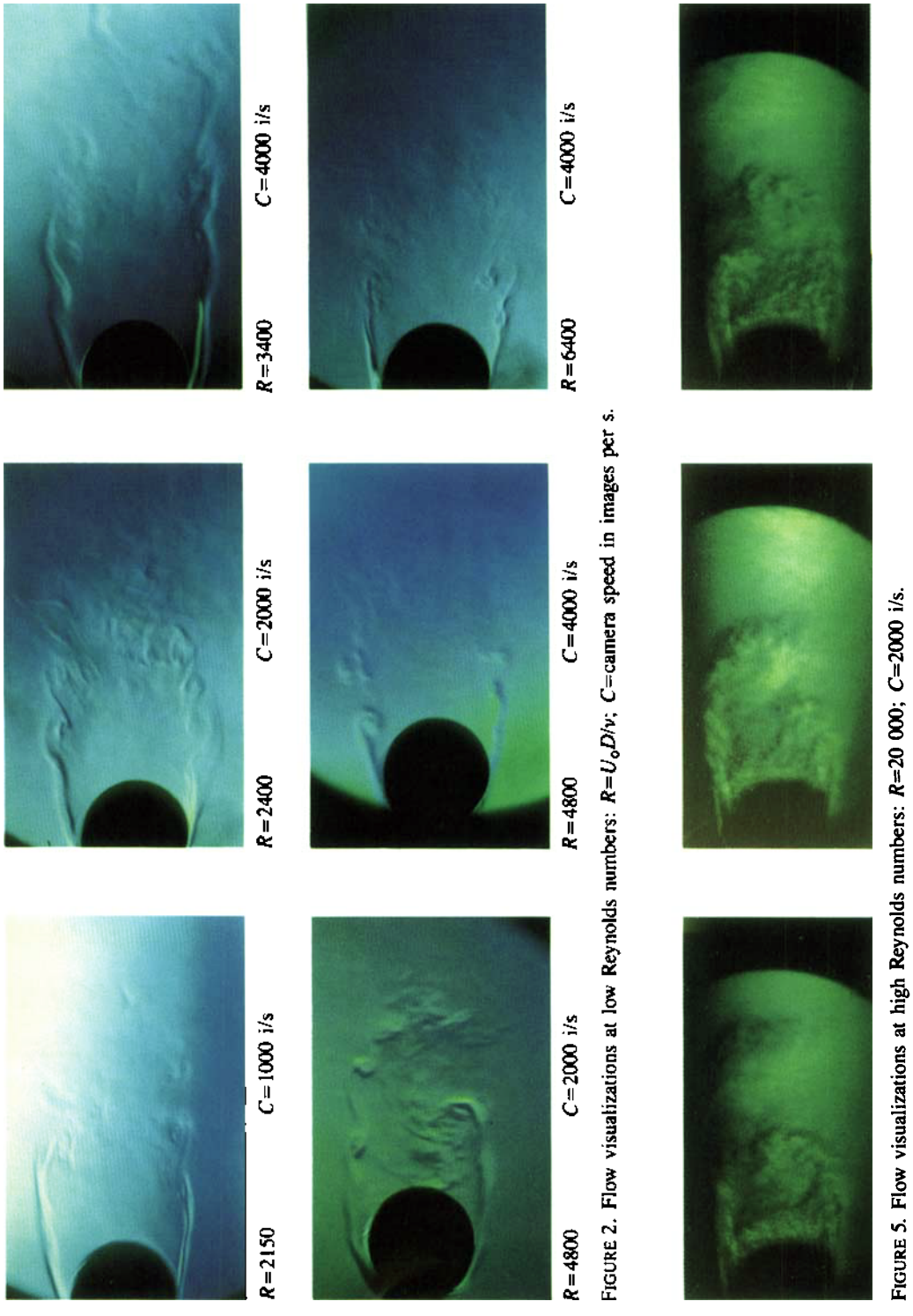

FIGURE 2. Flow visualizations at low Reynolds numbers: $R=U_0D/\nu$; C=camera speed in images per s.

FIGURE 5. Flow visualizations at high Reynolds numbers: R=20 000; C=2000 i/s.

from the main large vortices. The phase average of all the sample at a given phase with respect to the phase reference instant is defined as

$$\langle U(t)\rangle = \langle U\rangle(\tau) = \langle U\rangle(nT) = \frac{1}{M}\sum_{i=1}^{M} U(t-T_i+nT). \tag{1}$$

In this formula T_i is the phase reference as given by the reference probe, located in the non-turbulent external flow, τ is the time lag to T_i and corresponds to the phase angle $2\pi\tau/T_s$, T_s being the vortex-shedding period. T is the sampling period of the signal which is also maintained for the phase-average calculation.

Flow visualizations are conducted in an open tunnel of larger test section (diameter 2400 mm). The schlieren technique is used with high-speed camera frames. To obtain the necessary refraction-index contrast, the flow is seeded with carbon dioxide at the surface of the cylinder. Preliminary tests were carried out to ensure that the small inflow rate of tracer did not significantly change the nature of the flow and, in particular, the frequency response. Near the cylinder, the detailed structure of the small-scale vortices is observed as well as a general flapping of shear layers due to the large-scale vortex shedding. A sample of these visualizations is shown on the photographs of figure 2 (Plate 1). The observed frequency related to the crossing of the observed vortices was confirmed to be in agreement with those sensed locally by the hot-wire probes.

3. The experimental results

3.1. *Identification of two flow regimes*

In the lower Reynolds-number range ($2000 < R < 16000$), the flow visualizations of figure 2 show that the von Kármán vortices are not formed directly behind the cylinder. Between the back of the cylinder and the first appearance of the periodic vortex street, a dead-fluid zone is observed, bounded by two nearly parallel shear layers. The flow visualizations also show small-scale vortices which control the mixing-layer growth. Observations indicate that this mechanism is regular and seems to be periodic. It follows that these small vortices are carried by the larger regular vortices of the main vortex shedding, giving rise to the complex interaction mechanism of transition. In this case two different frequency sources are present as confirmed by the spectral measurements (see §3.3).

As the Reynolds number increases, the length of the dead-fluid zone decreases and the location of the first instability waves in the shear layer moves upstream. The visual approach provided by high-speed film allows a rough estimate of the lengthscales (figure 3) involved in this mechanism, which are given in table 1.

The conventional length of the formation region (L_f) can also be determined by the position of the maximum intensity of the fluctuation, on the centreline of the wake, as proposed by Bloor & Gerrard (1966). This length is found to decrease monotonically for $2000 < R < 16000$ (figure 4), confirming the flow-visualization results.

In the high Reynolds-number range ($16000 < R < 60000$), the dead-fluid zone is no longer detected and the vortices are formed directly at the back of the cylinder (figure 5, Plate 1). This gives rise to very large-amplitude fluctuations observed over the cylinder at $X/D = 0$. The 'fine-scale' vortices of the mixing layer merge into the von Kármán vortices which are carried away downstream through the non-turbulent external potential flow.

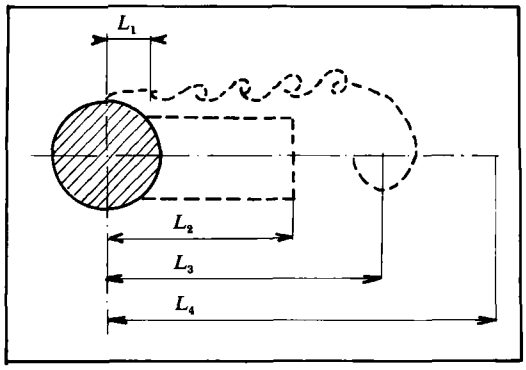

FIGURE 3. Schematic diagram of lengthscales.

R	L_1/D	L_2/D	L_3/D	L_4/D
2400	0.5	1.3	1.75	2.5
4800	0.45	1.0	1.26	2.1

TABLE 1. Different characteristic lengthscales: L_1, appearance of instability in the shear layer; L_2, length of the dead fluid zone; L_3, starting of the wake vortex; L_4, final length of the formation region

The probability density functions illustrate this point (figure 6). At $X/D = 0$ two zones, each characterized by a well-defined sharp single peak, are observed near the wall and in the external zone. From the bimodal distribution observed in the zone corresponding to the shear layer it is deduced, in agreement with the flow visualization, that this shear layer is subjected to an oscillating motion due to the direct effect of the large vortex. Thus the signal is typically the signature of an intermittent pattern marked by the alternating presence of the external flow and the small-scale vortices of the shear layer.

These features are very similar to those observed by Gerrard (1967) for $R = 20000$ and by Maekawa & Mizuno (1967) for $R = 10^5$ and are detailed in §3.5.

This first inspection of the mean properties of the flow clearly confirms the difference between the two flow configurations and suggests the need for a separate study with adequate methods for each regime.

3.2. *Relation between the frequency ratio and Reynolds number*

Two basic frequencies, f_s for vortex shedding and f_t for the mixing layer, can be clearly identified in the Reynolds-number range $2000 < R < 16000$ from the hot-wire measurements and confirmed by flow visualizations. The relationship between these frequencies is essential for understanding the interaction between both classes of vortices. It was derived first by Bloor (1964).

In the wake subcritical regime, the whole flow field in the vicinity of the cylinder is closely controlled by the vortex-shedding mechanism. Assuming that the corresponding characteristic timescale is imposed on all the terms of the momentum equation, and using the classical boundary-layer approximations, it can easily be

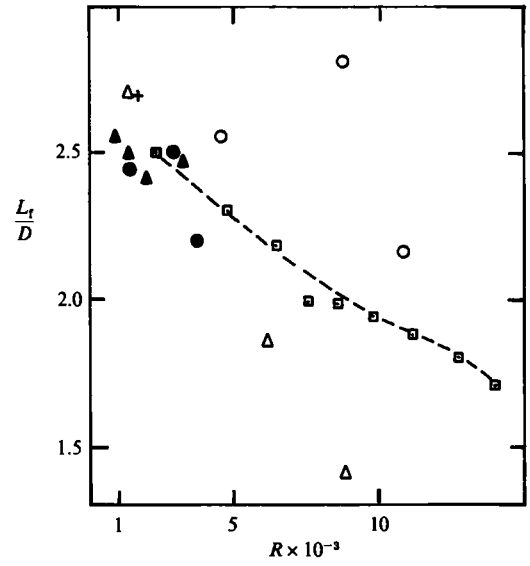

FIGURE 4. The length of the formation region. Bloor (1964): ○, $D = 1$ in.; △, $\frac{1}{4}$ in.; ●, $\frac{1}{10}$ in.; ▲, $\frac{1}{8}$ in.; +, $\frac{1}{16}$ in. Present study: ---⊡---, $D = 42$ mm.

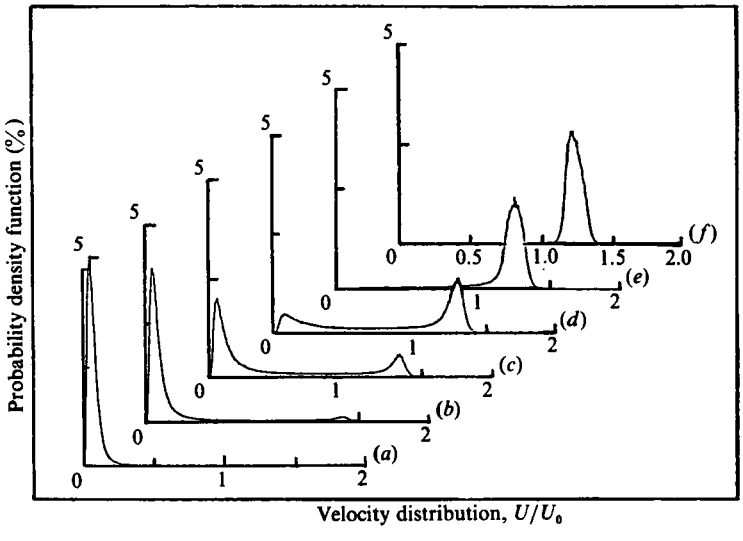

FIGURE 6. Probability density functions of the hot-wire signal at a Reynolds number of 56000 in section $X/D = 0$. (U is the amplitude of the velocity.) (*a*) $Y/D = 0.55$; (*b*) 0.5625; (*c*) 0.575; (*d*) 0.5875; (*e*) 0.6; (*f*) 0.6125.

inferred from an elementary analysis that the characteristic width scale δ of the mixing layer varies as

$$\frac{\delta}{D} \propto S^{-1} R^{-\frac{1}{2}}, \tag{2}$$

and

$$\frac{f_t}{f_s} \propto R^{\frac{1}{2}}, \tag{3}$$

with $S = f_s D/U_0$ and $R = U_0 D/\nu$.

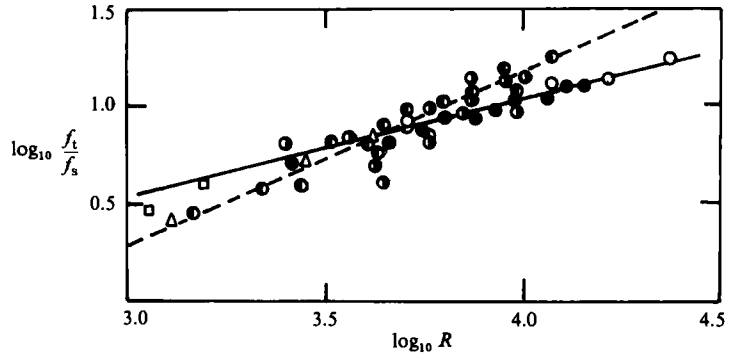

FIGURE 7. The frequency ratio as a function of the Reynolds number: △, ○, Bloor (1964); □, Gerrard (1978); ◑, ◐, Wei & Smith (1986); ●, present study; ——, $f_t/f_s \propto R^{\frac{1}{2}}$; – – –, $f_t/f_s \propto R^{0.87}$.

According to this analysis it turns out that if the Bloor (1964) relationship is verified, all timescales that have evolved from the momentum balance are controlled by the vortex-shedding one. The role of the pressure forces is merely to transmit the effect of the large-scale structures on the local development of the shear layer.

Contrary to these results, Wei & Smith (1986) have found that the ratio f_t/f_s is roughly proportional to the 0.87 power of the Reynolds number. They deduce that the rationale for this 0.87-power Reynolds-number dependence seems to lie in the fact that the instability frequency has its origin in a shear-layer instability. In this case, the location of the characteristic momentum thickness of the linear growth region, which fixes the frequency of the shear-layer vortices, moves towards the cylinder when the Reynolds number increases. Our analysis agrees with this suggestion but gives some evidence for the control of this phenomenon by the development of the boundary layer along the cylinder. Accordingly a 0.5 power law seems to be adequate as suggested in figure 7.

In figure 7 we report all the results from Bloor (1964), Gerrard (1978) and Wei & Smith (1986), in addition to those of the present study. Reasonable agreement can be observed with the following formula

$$\frac{f_t}{f_s} = 0.095\, R^{\frac{1}{2}} \quad \text{for } 2000 < R < 16000,$$

suggested first by Bloor (1964).

The details of the interaction between both scales of vortices are provided in §§3.3 and 3.4. Because experimental information on the fluctuating pressure field is not available, the use of pressure–velocity method to perform the numerical simulation (§4) is considered adequate to describe the main features of this interaction in order to point out the role of the pressure. The timescale $T_0 = 1/f_s$ will be superimposed as an external forcing on the natural development of an idealized shear layer, sketching the gross features of the main coupling mechanism.

At higher Reynolds number, the frequency ratio increases so that the previous characteristic scales become uncoupled. Owing to this distinction, the corresponding flow regime will be studied by different methods (§3.5).

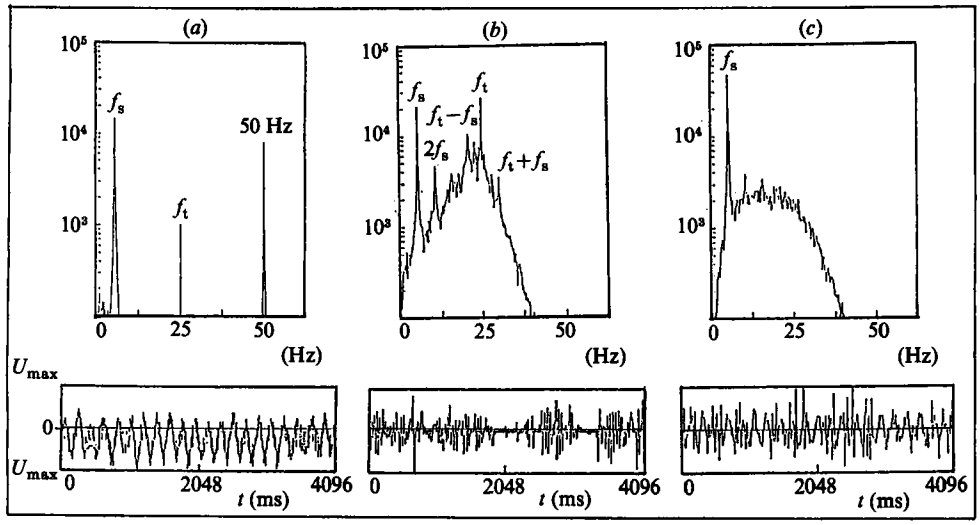

FIGURE 8. Power spectra and traces in the shear layer; $Y/D = 0.625$, $R = 2660$. (*a*) $X/D = 0.125$; (*b*) 1.375; (*c*) 3.525 (arbitrary scales).

3.3. *Vortex interaction in the low-Reynolds-number range*

Over the range of Reynolds numbers $2000 < R < 16000$, and as shown by flow visualizations, the power spectra exhibit the same characteristics as those given in figure 8 for $R = 2660$. Near the cylinder (figure 8*a*), two peaks appear corresponding to the shear-layer frequency f_t, and to the wake vortex-shedding frequency f_s. Moving downstream, as the peak corresponding to f_t increases (figure 8*b*), coupling phenomena between f_t and f_s are apparent. Sideband peaks at the sum and difference of f_t and f_s appear. The occurrence of these frequencies ($f_\nu = f_t - f_s$ and $f_\sigma = f_t + f_s$) is caused by the non-linear interaction between the shear layer and the vortex street (Miksad *et al.* 1982).

At the end of the interaction zone ($X/D > 2.5$), only the peak at f_s is observed in the spectrum and the initially organized shear layer has lost its periodic character (figure 8*c*). The spectrum reveals the superposition of random motion on the pseudoperiodic components (f_s and its harmonics). The situation is then the one observed in the convected wake by Boisson *et al.* (1981) (see also Boisson 1982).

In order to quantify the development of the different components, the longitudinal variations of the amount of spectral power corresponding to different frequency bands are compared to the total power of each spectrum. The amount of power corresponding to a peak in the spectrum is calculated by subtracting the random contribution from the total spectral area in the given band. The purpose here is to show the spectral transfers between different bands. The information on the power content is approximate and only provide a rough description of the situation. Figure 9 displays the contribution of the vortex-shedding phenomenon, i.e. the power in the narrow band around f_s, that of the shear-layer vortices around f_t, the amount of power involved in the interaction process in the narrow bands around f_ν and f_σ, and the total fluctuating power $\overline{u^2}$ obtained by integration over the whole spectrum.

Interpreting these figures, three different zones can be distinguished. In the first one ($X/D < 0.5$) the total power is nearly constant and the main contribution is due to the oscillations of the vortex shedding. For f_t and f_ν, the power is rapidly increasing

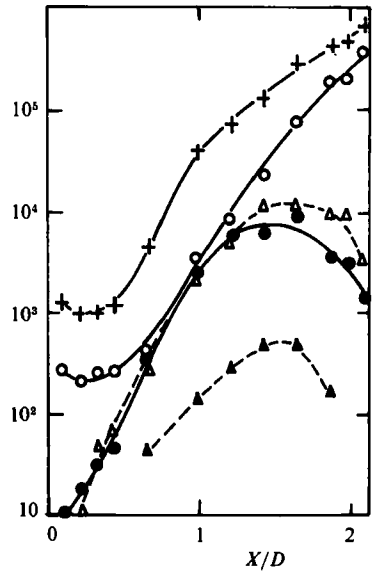

FIGURE 9. Longitudinal evolution of power spectra; $Y/D = 0.625$; $R = 2660$ (arbitrary scales): +, total power; ○, f_s; ●, f_t; △, f_ν; ▲, f_σ.

but, in fact, corresponds to a very low level. Moving downstream, a strong increase of all the previously listed contributions is observed up to approximately $X/D = 1.2$. The amount of power corresponding to the three frequencies f_s, f_t and f_ν is roughly the same. This reveals the first stages of the increasing strong nonlinear interaction process between the small-scale vortices and the larger ones. It can be noticed that a similar trend is observed for the spectral component at the frequency f_σ, which is however much less important than the others. For $X/D > 1.2$, while the total intensity and that of the vortex shedding increase monotonically, the components at f_t, f_ν and f_σ reach a maximum and then decrease, the power at f_ν becoming larger than that at f_t. Finally, the vortex-shedding frequency becomes predominant and the remaining fluctuations are random. The organized character of the shear layer tends to be smeared out by the disorder introduced in the roll-up process of the smaller vortices convected by the bigger ones.

The process described above is not currently observed in free-shear layers. It involves a destabilization of the three frequencies f_s, f_t and f_ν. Such intermodulations were described by Motohashi (1979) and Miksad *et al.* (1982), who observed that a system of two frequencies which becomes a system with three frequencies, leads to the development of complicated sideband structures attributed to amplitude and phase modulation, involving successive sums and differences of the existing peaks. Hence a growing number of interacting frequencies is created at $f_t \pm nf_s$ resulting in a broadening of the initial spectrum. Figure 10(*a*) shows the longitudinal evolution of the spectra in the mixing layer at the maximal intensity point ($Y/D = 0.625$). Coupling phenomena corresponding with the last description are apparent on this figure.

It can also be noticed that the background level of the random fluctuations grows in the preferred bandwidth (f_s,f_t) where the interaction takes place. This feature enhances the role played by the interaction of both two-dimensional processes in the establishment of a final turbulent state (figure 10*a*).

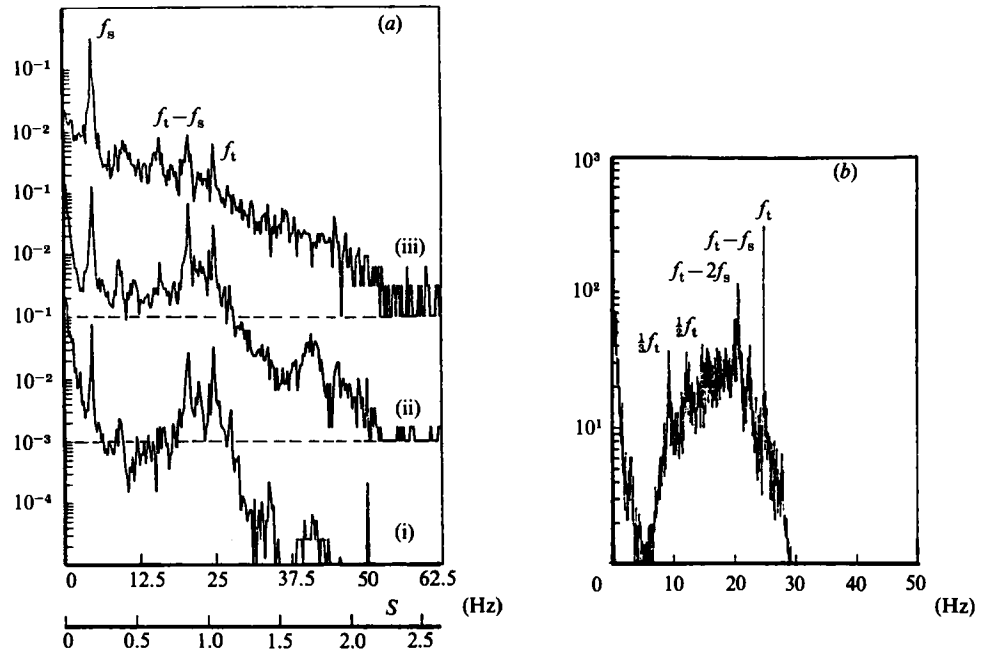

FIGURE 10. Normalized power spectra of velocity at $Y/D = 0.625$, $R = 2660$. (*a*) Flow without splitter plate: $df = 0.244$ Hz; (i) $X/D = 1$; (ii) 1.4; (iii) 2. (*b*) With splitter plate: $df = 0.05$ Hz, $X/D = 1$.

3.4. *Effects of a splitter plate*

A splitter plate is introduced in these experiments in order to investigate the possible connection between the frequency f_t of the shear layer and the vortex-shedding frequency. Experiments reported by several authors, such as Roshko (1954), Gerrard (1966, 1978), Apelt *et al.* (1973), have shown that the features of the separated wake downstream of a cylinder can be greatly affected by a splitter plate placed along the centreline of the wake. For Reynolds numbers at which a regular vortex street is shed from the cylinder, the vortex shedding may be altered or even suppressed and the drag force modified. In particular, it has been found that as the splitter plate length is increased, the Strouhal number is decreased and the pressure drag reduced. 'Long' plates inhibit interaction between the separated shear layers, and near the cylinder conditions are much steadier than with short plates (or without a plate).

In the present study, a $4.12D$ long splitter plate, placed along the centreline of the wake at the back of the cylinder, stabilizes the flow behind the cylinder, and prevents it from direct interaction between both sides. The Strouhal number S is found to be quite independent of the Reynolds number and equal to

$$S = f_s \frac{D}{U_0} = 0.13 \pm 0.004.$$

For $R = 4800$, the pressure drag is reduced to 75% in agreement with the results of Roshko (1955). Preliminary measurements show that the r.m.s. pressure fluctuation is reduced by at least 80% and the mean flow is modified because the position of the separation point is different and corresponds to an angle of 70° from the front stagnation point.

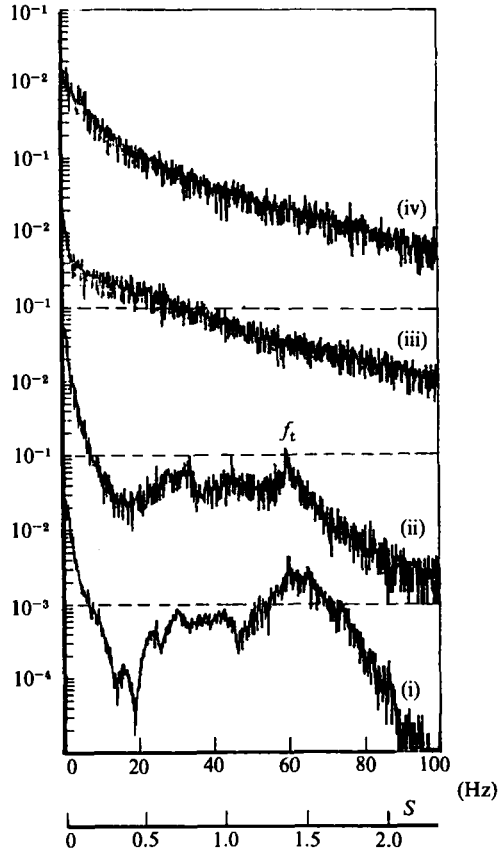

FIGURE 11. Normalized power spectra of velocity with a splitter plate; $R = 4800$; $Y/D = 0.786$; $df = 0.0976$ Hz: (i) $X/D = 0.59$; (ii) 1.0; (iii) 3.0; (iv) 5.0.

Despite a strong attenuation, it has been verified that the vortex-shedding process still took place and was clearly observable downstream of the plate and in the potential flow. Accordingly the impact of this periodic phenomenon is much weaker than without a splitter plate near the cylinder wall and in the shear layers. In fact, a subharmonic at $\frac{1}{2}f_t$ is observed. This is typically associated with the pairing process as described by Ho & Huerre (1984), among others, for the plane mixing layer. However, in the shear-layer region, an interaction with the vortex shedding, though weaker than without the plate, still exists as observed by the $(f_t - f_s)$ frequency peak (figure 10*b*). Also observable are higher-order subharmonics $\frac{1}{3}f_t$, $\frac{1}{4}f_t$, as a consequence of the nonlinearity process. The interaction between these subharmonics and the principal frequency leads to the appearance of $(1-1/n)f_t$ frequencies. At the same time the background level of the random fluctuations, initially centred on the mixing-layer frequency, spreads over a broader band and finally extends to the whole spectrum.

In the shear layer developing downstream of the cylinder and nearly parallel to the uniform flow direction, the intensity of the fluctuations rises considerably. A maximum is found near the line $Y/D = 0.79$, the typical spectra for which are given on figure 11 for $R = 4800$. In this case, the width of the wake is larger than without the splitter plate. The vortex-shedding frequency peak cannot be distinguished in the

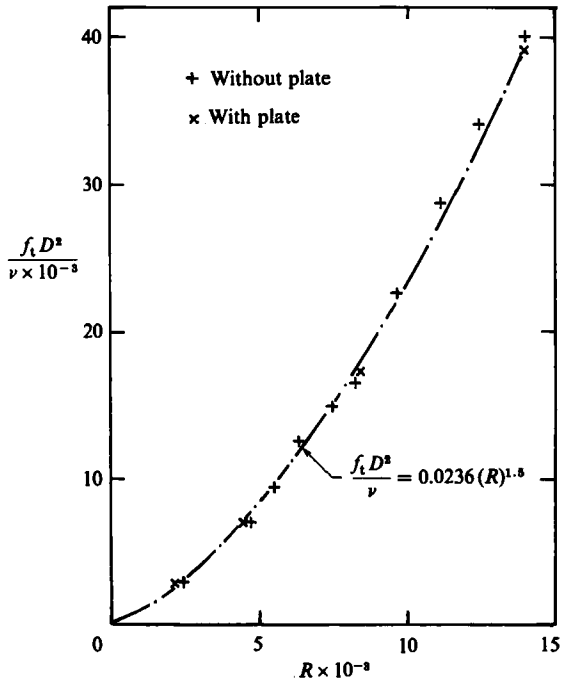

FIGURE 12. Non-dimensional variations of the frequency f_t with respect to the Reynolds number.

first stage of the development of the shear layer (namely $X/D < 1$). But a discrete peak is found at the frequency f_t of the shear-layer vortices, which is very close to that occurring at the same corresponding Reynolds numbers without the splitter plate, as shown in figure 12.

In both cases (with and without the plate) the frequency follows the non-dimensional relationship

$$\frac{f_t D^2}{\nu} = 0.0236 R^{\frac{3}{2}}.$$

For constant cylinder diameter, the frequency f_t is thus proportional to $U^{\frac{3}{2}}$, as observed by Bloor (1964) in the case without a plate (see figure 3 of that reference).

In these cases the frequency f_t depends only on the cylinder Reynolds number and is a local feature of the shear layer. There is no significant effect of a variation in the vortex-shedding process associated with a different frequency f_s. The shear layer develops its own independent instabilities disconnected from the vortex shedding despite the location of the separation point further upstream and of the larger wake width in the case with the splitter plate. This seems to exclude a feedback mechanism in the establishment of this frequency.

3.5. *The intermittent regime at high Reynolds number*

As mentioned in §3.1, within the Reynolds-number range $16000 < R < 60000$, the flow is marked by high fluctuation levels near the wall of the cylinder, and particularly at $X/D = 0$. The spectra are, in this case, of the pseudoperiodic type, i.e. constituted by rather sharp peaks at f_s and its harmonics and a smooth distribution attributed to random small-scale motions (figure 13). The power corresponding to the frequency

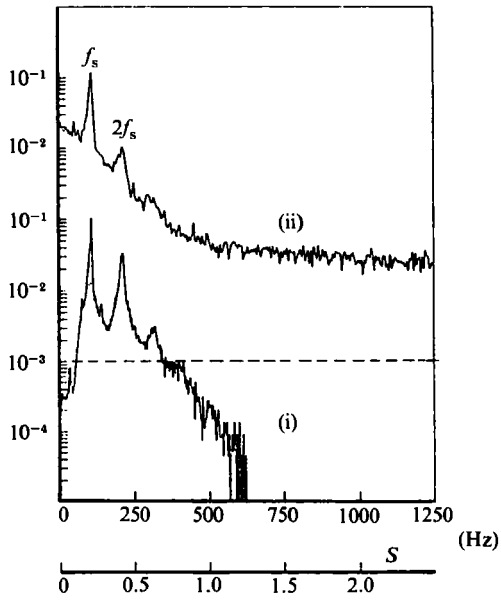

FIGURE 13. Normalized power spectra of velocity at $Y/D = 0.575$; $R = 56000$; $df = 4.88$ Hz: (i) $X/D = 0$; (ii) $X/D = 0.25$.

given by Bloor's (1964) formula is negligible on the measured spectra. It turns out that the zone where the regular vortices of the shear layer are formed is located closer to the separation point and that this motion is rapidly disorganized.

As observed on the recorded velocity traces obtained in the present study, which agree nicely with the results of Gerrard (1967) and of Maekawa & Mizuno (1967, figure 2), a period has smooth portions corresponding to the crossing of potential flow and fine-scale turbulence from the wall boundary layer.

In order to educe the organized pseudoperiodic signal from the random background, phase averaging (§2) was performed using the approach of Boisson *et al.* (1983).

The phase-averaged traces of the velocity signal in section $X/D = 0$, represented on figure 14(*a*), are all nearly periodic at f_s. A high level of organized fluctuation is found in the central region of the mixing layer where the trace is nearly symmetrical in a period. Two low-fluctuation zones are observed around this position. The first one for high velocity in the potential flow is almost sinusoidal and reflects induced oscillations. In the second zone, near the wall, the phase-averaged signal has only one amplitude bump in a period, which is due to the influence of the potential flow on the low-velocity wall region. The corresponding bimodal amplitude histograms for the same lateral position are in good agreement with these traces, which confirms that the intermittent character of the fluctuation is mainly controlled by the organized motion at the Strouhal frequency.

A correct description of the motion in the zone near the cylinder is obtained by plotting the phase-averaged velocity profiles (figure 14*b*). These are calculated, for a given phase angle, by adding the value of the phase-averaged fluctuation to the mean velocity profile. These profiles are typically those of a flapping motion of the shear layer. The maximum of the amplitude fluctuation is located near the inflexion point of the mean velocity profile but inflexion points of individual profiles move in

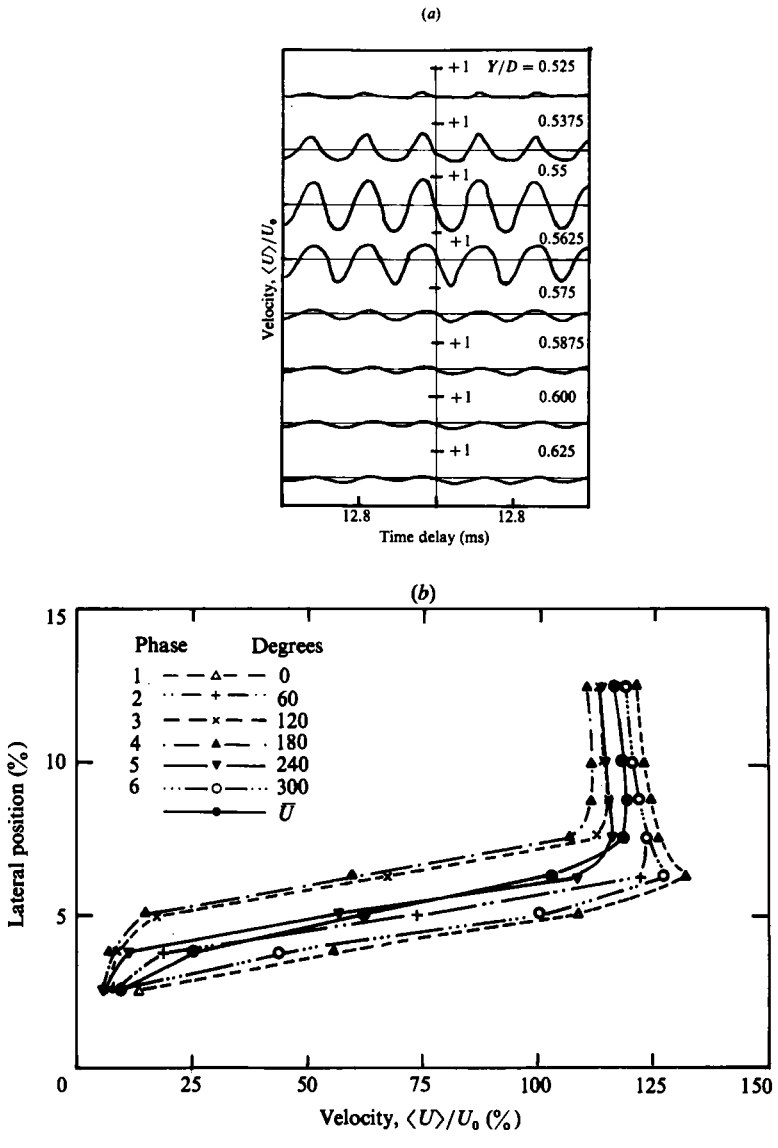

FIGURE 14. (*a*) Phase-averaged traces of the hot-wire signal; (*b*) phase-averaged velocity profiles ($R = 56000$; $X/D = 0$).

space with the phase angle. One should notice also that the local acceleration is maximum near the phase zero. In this position the velocity fluctuation is also maximum and the potential flow penetrates more deeply towards the wall.

This description shows that the small-scale internal motion is likely to play a secondary role in the global fluctuation, which is mainly of an organized type in this range of Reynolds numbers. In this case both scales are uncoupled and the small-scale motion can be considered as acting through some type of 'eddy viscosity'.

4. Study of the governing mechanism

4.1. *Links between the experiments and numerical simulations*

The experimental analysis shows the importance of the non-linear interaction in the transition zone observed for the strong-interaction regime (lower Reynolds numbers). In order to analyse separately the dynamics of the mixing-layer eddies and the interaction mechanism with the alternating ones, a two-dimensional unsteady mixing-layer flow is computed by direct solving of the time-dependent Navier–Stokes equations.

Here, the aim is not to describe the flow around a circular cylinder but to simulate the interaction between the two different-scale vortices in the actual mixing layer.

The simplified flow studied is a plane mixing layer that develops from the merging of two streams that are initially parallel.

The control parameters that can influence the dynamic of the shear layer are: (i) the velocity ratio $r = (U_1 - U_2)/(U_1 + U_2)$ $(U_1 > U_2)$; (ii) the Reynolds number $R' = U_1 b_0/\nu$, where b_0 is approximately the initial width of the mixing layer; and (iii) the initial laminar or turbulent state of the boundary layers before the merging.

According to Ho & Huerre (1984), the variation of the natural frequency f_t changes by only 5% between $r = 0$ and $r = 1$. In the case of the cylinder, our measurements do not allow an accurate determination of the value of r but, owing to the weak influence of this parameter on the frequency f_t, it was arbitrarily fixed at a value $r = 0.33$.

A large Reynolds-number range (R') was covered, from 200 to 1000, in order to remain in the initial laminar-boundary-layer regime as for the cylinder in the subcritical regime. Furthermore, the transition to turbulence in the initial layer is obtained for a Reynolds number greater than 10^3 as reported by Ho & Huerre (1984).

In this case, the Reynolds number takes into account the main phenomena concerning the frequency evolution. Rough estimates of the width of the cylinder shear layer show that the actual Reynolds number ($R = U_0 D/\nu$) for the wake is related to the Reynolds number ($R' = U_1 b_0/\nu$) of the shear layer by $R = 10R'$.

The numerical method is that developed by Braza (1981) and Braza, Chassaing & Ha Minh (1986). It applies to the two-dimensional and unsteady cases. Details concerning the numerical method can be found in Kourta (1984). In the following, the non-dimensional space coordinates X and Y are expressed with respect to the mesh size.

4.2. *Results*

The discussion of the results is twofold: analysis of natural instabilities of the mixing-layer structures; and analysis of the nonlinear interaction.

The basic mechanisms governing the development of mixing layers are pointed out with the help of streaklines (figure 15). This development is initially dominated by a linear instability mechanism. The streaklines issuing from the upstream section show that at first the flow is steady. All lines are parallel in this zone. Farther downstream, instability waves are detected. The exponential growth leads finally to the roll-up process, which is found to be periodic at the fundamental frequency f_t.

In order to estimate quantitatively the growth of the mixing layer, the expansion is defined by the streamlines corresponding to $U = 0.95U_1$ and $U = 1.05U_2$. The results are plotted for a Reynolds number of 200 in figure 16, which shows a good agreement with the analytical law (Liepmann & Laufer 1947) for the laminar case. Indeed, in the first region ($X < 20$), the spread can be written as

$$b = kX^{\frac{1}{2}}.$$

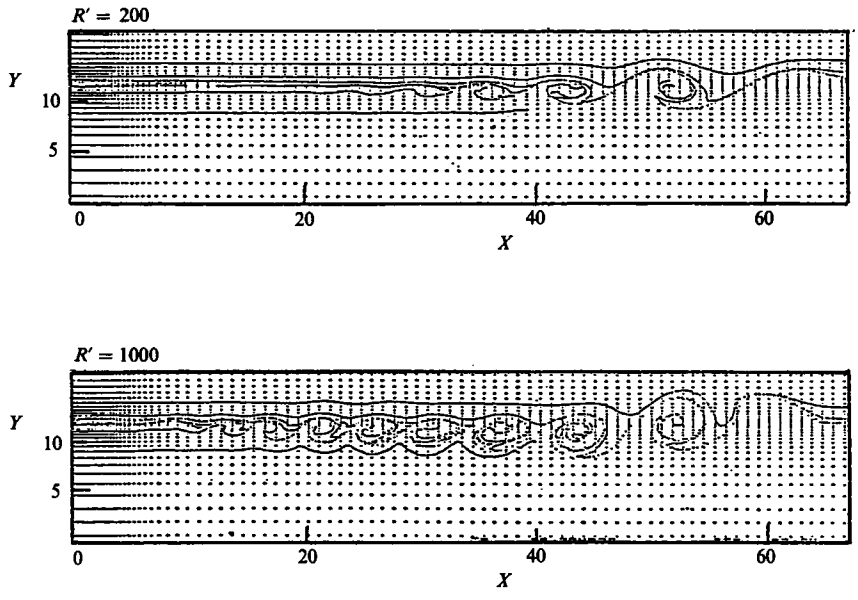

FIGURE 15. Streakline patterns at different Reynolds numbers (natural mixing layer).

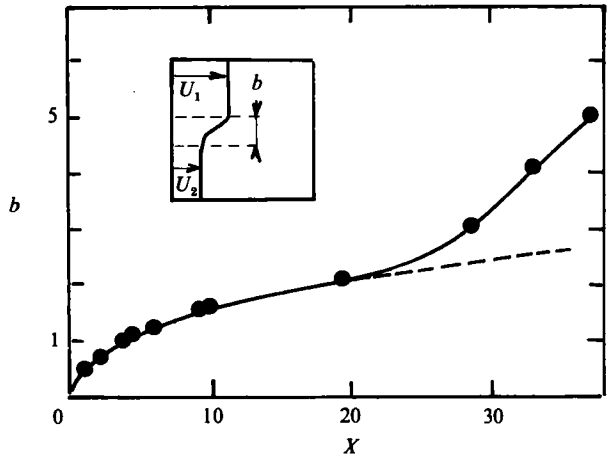

FIGURE 16. The spread of the mixing layer: ----, $b = kX^{\frac{1}{2}}$.

It can also be seen that beyond $X = 28$ the spread becomes approximately linear after a transition zone situated in the interval $20 < X < 28$.

As the Reynolds number increases, the setting up of the instability is found to occur earlier and the fundamental frequency f_t increases. The corresponding shear-layer Strouhal number $S' = f_t b_0 / U_1$ is given in table 2. The initial width b_0 is evaluated from the extrapolation of the curves $b = f(X)$ near the inlet section and found equal to 0.5 ± 0.05 for the three Reynolds numbers explored.

In order to simulate the vortex-shedding excitation of the shear layer in the wake of a circular cylinder, a forcing mechanism is introduced.

In this paper, the mixing layer is excited at $\frac{1}{2}f_t$ and at f_t/a (a being a non-integer

R'	200	500	1000
S'	0.046	0.065	0.075

TABLE 2. Variation of S' with R'

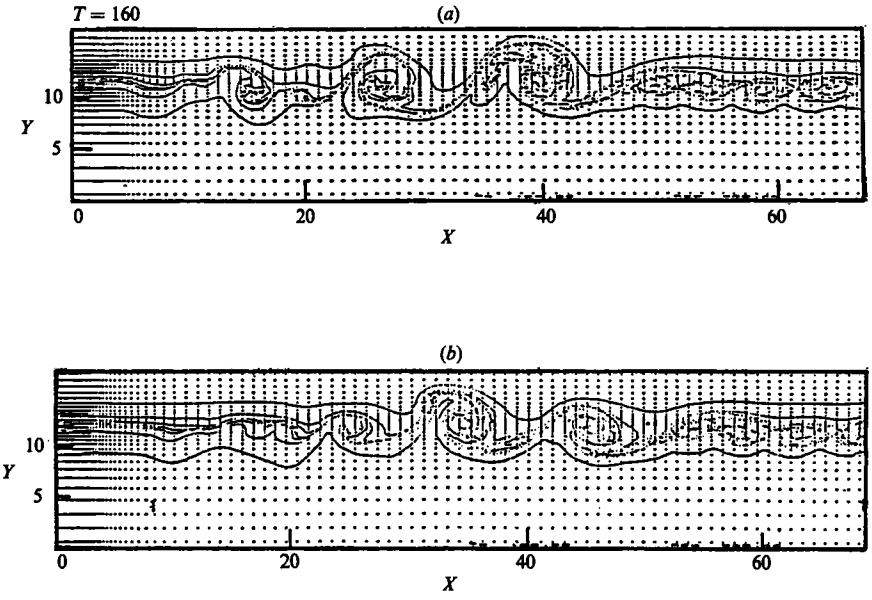

FIGURE 17. Numerical simulation of the excited layer: (*a*) a forcing at $\frac{1}{2}f_t$; (*b*) a forcing at $f_t/6.94$.

equal here to 6.94). The forcing is applied in the inlet section by varying the direction of the velocity at the inflexion point. This type of excitation seems to be adequate for the Reynolds-number range investigated ($2000 < R = U_0 D/\nu < 16000$) and for the initial domain addressed. Indeed, the flow visualizations show that the shear layers are nearly parallel to the flow direction and the effect of the shedding is essentially to tilt the initial flow across this direction.

The sensitivity of a shear layer to initial conditions from the effects of a varying forcing frequency f_f was studied by Ho & Huang (1982). They have shown that in the range ($\frac{1}{2}f_t < f_f < 2f_t$), the initial vortex-formation frequency f_r is equal to f_f. For the lower forcing frequencies ($\frac{1}{4}f_t < f_f < \frac{1}{2}f_t$), the response frequency f_r jumps to the first harmonic $2f_f$ and vortex pairing is promoted.

In the first case of the present study, forcing at the first subharmonic is chosen because of its importance in the pairing mechanism as observed experimentally by Freymuth (1966) and Ho & Huerre (1984).

When the forcing is applied, the neighbouring vortices are laterally displaced, owing to different convective velocities, and wrap around each other to form a single structure in the classical pairing process (figure 17*a*). The roll-up process is completed at the station where the component at f_r (the response frequency) reaches its maximum. The spreading of the shear layer is therefore increased by the occurrence of pairing. This interaction is observed in a transient phase after which the forcing

controls the shedding frequency. The emitted vortices are twice as big as the natural ones and are shed at a frequency of $\frac{1}{2}f_t$.

Such a pairing process is observed in several flow regimes in the shear layer emerging from the cylinder, and especially when a splitter plate is added. In this case, it becomes the predominant process in the coupling mechanism.

The last case simulated is the forcing at frequency (f_t/a). This excitation is superimposed to simulate the chopping effect of the alternating-eddies frequency on the mixing layer. In this sample configuration a nonlinear interaction between the above frequencies is observed. The forcing frequency is chosen to be equal to $f_t/6.94$, which corresponds past the cylinder to a vortex shedding frequency f_s for Reynolds number $R = 5000$. A strong coupling exists then between both vortical motions.

The effect of this forcing is shown on figure 17 (*b*). Vortex pairing is also observable but, in contrast with the previous case, this mechanism is irregular. Single vortices at the natural frequency can be found among those forming pairs and the spectrum is likely to contain a complex set of the interaction frequencies as is observed in the case of the formation zone of the wake of the cylinder. Indeed the interaction frequencies can be detected. The time-dependent pressure oscillates at a frequency of $(\frac{1}{2}f_t - f_t)$ and the V-component at $(f_t - f_t)$, which was found to be predominant in the case of the cylinder (Kourta *et al.* 1985*a*).

5. Discussion and conclusion

Evidence has been given for the existence of two different types of interaction between the vortex shedding and the 'small-scale' structures in the transition process in the near wake of a cylinder. The scale ratio between both vortical phenomena is shown to have a large influence on the flow regimes.

For the lower Reynolds-number range ($2000 < R < 16000$) the frequencies of both phenomena are of same order and induce strong interactions governing the flow pattern near the cylinder. On the other hand, when R is large enough ($16000 < R < 60000$), the two frequency ranges are disconnected and the small vortices seem to act as an eddy viscosity.

The strong-interaction regime (lower Reynolds numbers) is mainly dominated by the response of the separated shear layer to the forced frequency of the vortex shedding. In this case, indeed, the flow geometry includes a dead-fluid zone bounded by a thin shear layer. Based upon such features, a timescale analysis leads to the Bloor's (1964) relationship between both frequencies f_t and f_s. This unsteady process leads to the successive occurrences of sum and difference frequencies $f_t \pm nf_s$ in the power spectrum. These observed interaction frequencies are characteristic of a nonlinear interaction due to phase and amplitude modulations.

Such conclusions are reinforced by the results obtained from the experiments with a wake splitter plate where the two basic frequencies are discoupled. Two major observations seem to emerge. First, the frequency of the small-scale shear-layer vortices is unchanged while the main wake vortex shedding and all the mean flow properties are modified. This implies that in the previous case, both instability sources are independent. The second point is that a different process of instability is observed in the shear layer with the splitter plate. It appears that the subharmonic interaction pattern is more efficient than the interaction with the vortex shedding. In this case the development of the shear layer is similar to the classical two-dimensional mixing

layer involving the vortex-pairing mechanism, and the influence of the large vortices, formed at the back of the plate, is weaker.

The numerical simulation of the plane mixing layer both in the non-excited and in the excited case allows the determination of the principal features of the small-scale vortices when submitted to the external excitation due to the wake large structures. Such simulations confirm the major influence of two-dimensional effects on the transition to turbulence for this type of flow.

In the higher Reynolds-number range, the flow is found to be intermittent. The bimodal probability density functions, even in the wall vicinity as for $X/D = 0$, show the flapping motion of the shear layer, confirmed by the phase-averaged approach. It follows that the shear layer experiences large-amplitude oscillations at the vortex-shedding frequencies which are globally insensitive to the details of the small-scale disorganized vortices. The whole problem can be treated in this case as the unsteady organized intermittent pattern between the external non-turbulent and the vortical internal motions.

We wish to thank Professor G. S. West for providing helpful suggestions during a long stay in our laboratory and Dr M. Braza for valuable discussions. We would also like to thank Mr J. Bonnefont, Mr J. C. Pons and Mrs M. C. Nguyen-Tristani for their technical assistance. This work was supported by the French Army Department under contract number DRET 84/1412/DS/SR.

REFERENCES

Apelt, C. J., West, G. S. & Szewczyk, A. A. 1973 *J. Fluid Mech.* **61**, 187.

Bearman, P. W. 1965 *J. Fluid Mech.* **21**, 241.

Bloor, M. S. 1964 *J. Fluid Mech.* **19**, 290.

Bloor, M. S. & Gerrard, J. H. 1966 *Proc. R. Soc. Lond.* A **294**, 319.

Boisson, H. C. 1982 Développement de structures organisées turbulentes à travers l'exemple d'un cylindre circulaire. Thèse de Docteur ès-Sciences, I.N.P. Toulouse.

Boisson, H. C., Chassaing, P. & Ha Minh, H. 1983 *Phys. Fluids* **26**, 653.

Boisson, H. C., Chassaing, P., Ha Minh, H. & Sevrain, A. 1981 In *Unsteady Turbulent Shear Flows* (ed. R. Michel, J. Cousteix & R. Houdeville), p. 262. Springer.

Braza, M. 1981 Simulation numérique du décollement instationnaire externe par une formulation vitesse-pression. Application à l'écoulement autour d'un cylindre. Thèse de Docteur-Ingénieur, I.N.P. Toulouse.

Braza, M., Chassaing, P. & Ha Minh, H. 1986 *J. Fluid Mech.* **165**, 79.

Busse, F. H. 1981 *Hydrodynamics Instabilities and the Transition to Turbulence* (ed. H. L. Swinney & J. P. Gollub). Topics in Applied Physics. vol. 45, p. 96. Springer.

Cantwell, B. J. 1976 A flying hot-wire study of the turbulent mean wake of a circular cylinder at a Reynolds number 140000. Ph.D. Thesis, Caltech.

Crausse, E. 1936 Contribution expérimentale à l'étude de phénomènes transitoires et périodiques se produisant dans les lignes en mouvement. Thèse de Docteur ès-Sciences, Université de Toulouse.

Di Prima, R. C. & Swinney, H. L. 1981 *Hydrodynamics Instabilities and the Transition to Turbulence* (ed. H. L. Swinney & J. P. Gollub). Topics in Applied Physics, vol. 45, p. 139. Springer.

Domptail, C. 1979 Sillages turbulents en aval d'un ou de deux barreaux paralleles en tunnel hydrodynamique: visualisation et vélocimetrie laser. Thèse de 3e cycle, Université d'Aix-Marseille II.

Eckmann, J.-P. 1981 *Rev. Med. Phys.* **53**, 643.

FREYMUTH, P. 1966 *J. Fluid Mech.* **25**, 683.

GERRARD, J. H. 1966 *J. Fluid Mech.* **25**, 401.

GERRARD, J. H. 1967 *Phys. Fluids Suppl.* **10**, S98.

GERRARD, J. H. 1978 *Phil. Trans. R. Soc. Lond.* A **288**, 351.

HO, C. M. & HUANG, L. S. 1982 *J. Fluid Mech.* **119**, 443.

HO, C. M. & HUERRE, P. 1984 *Ann. Rev. Fluid Mech.* **16**, 365.

JONES, G. S., BARBI, C. & TELIONIS, P. 1981 Unsteady turbulent shear flows (ed. R. Michel, J. Cousteix & R. Houdeville), p. 228. Springer.

KOURTA, A. 1984 Analyse physique et simulation numérique des structures tourbillonnaires du sillage proche d'un cylindre circulaire. Thèse de Docteur-Ingénieur, I.N.P. Toulouse.

KOURTA, A., BOISSON, H. C., BRAZA, M., CHASSAING, P. & HA MINH, H. 1985*a* *Fifth Symp. on Turbulent Shear Flows. Cornell University, Ithaca, New York, USA*, p. 3.39.

KOURTA, A., BOISSON, H. C., CHASSAING, P. & HA MINH, H. 1985*b* *Intl J. Phys.-Chem. Hydrodyn.* **6**, 703.

KOVASZNAY, L. S. G. 1959 *J. Fluid Mech.* **6**, 357.

LIEPMANN, H. W. & LAUFER, J. 1947 *NACA Tech. Note* 1257.

MAEKAWA, T. & MIZUNO, S. 1967 *Phys. Fluids Suppl.* **10**, S184.

MIKSAD, R. W., JONES, F. L., POWERS, E. J., KIM, Y. C. & KHADRA, L. 1982 *J. Fluid Mech.* **123**, 1.

MOTOHASHI, T. 1979 *Phys. Fluids* **22**, 1212.

NEWHOUSE, S., RUELLE, D. & TAKENS, F. 1978 *Communs Math. Phys.* **64**, 35.

OWEN, F. K. & JOHNSON, D. A. 1980 *AIAAJ.* **18**, 1173.

ROSHKO, A. 1954 *NACA Rep.* 1191.

ROSHKO, A. 1955 *J. Aero. Sci.* **22**, 124.

SIROVICH, L. 1985 *Phys. Fluids* **28**, 2723.

SREENIVASAN, K. R. 1985 In *Frontiers in Fluid Mechanics* (ed. S. H. Davis & J. L. Lumley), p. 41. Springer.

STANSBY, P. K. 1974 *Aeronaut. J.* **78**, 36.

WEI, T. & SMITH, C. R. 1986 *J. Fluid Mech.* **169**, 513.

WEST, G. S. & APELT, C. J. 1982 *J. Fluid Mech.* **114**, 361.

WLEZIEN, R. W. & WAY, J. L. 1979 *AIAAJ.* **17**, 563.